Contribution from the Department of Chemistry, Northwestern University, Evanston, Illinois 60208, and Exxon Research and Engineering Company, Annandale, New Jersey 08801

Synthesis and Molecular and Electronic Structure of Stable Salts Containing the Radical Anions $[Fe_4(CO)_{12}CC(O)R]^{2-}$ (R = CH_3, $CH_2C_6H_5$)

Jiandang Wang,† Ann M. Crespi,† Michal Sabat,† Suzanne Harris,*,‡ Carrie Woodcock,† and Duward F. Shriver*,†

Received August 30, 1988

The cyclic voltammograms and bulk electrolysis of $[PPN][Fe_4(CO)_{12}CC(O)R]$ (**2a**, R = Me; **2b**, R = CH_2Ph; $[PPN]^+$ = $[(Ph_3P)_2N]^+$) demonstrate a surprisingly favorable one-electron reduction to produce **3**, which contains a stable dinegative radical cluster anion, $[PPN]_2[Fe_4(CO)_{12}CC(O)R]$ (**3a**, R = Me; **3b**, R = CH_2Ph). EPR spectra of **3** indicate that the odd electron is on the iron carbonyl cluster and is not delocalized onto the CC(O)R ligand. Chemical reduction of **2** with Na/Hg leads to an almost quantitative generation of **3**, which can be isolated as the $[PPN]^+$ salts **3a** and **3b** or $[Me_3NCH_2Ph]_2[Fe_4(CO)_{12}CC(O)Me]$ (**3c**). A single-crystal structure determination of **3c** confirms the presence of a butterfly Fe_4 cluster anion with the CC(O)Me group bonded to all four iron atoms. Detailed comparisons between structures of **3c** and **2a** and Fenske–Hall MO calculations indicate that the added electron in **3** resides in a metal-framework-based orbital that is weakly antibonding between the hinge and wingtip Fe atoms. Crystal data for **3c**: triclinic, $P\bar{1}$, a = 12.242 (2) Å, b = 14.904 (3) Å, c = 11.704 (2) Å, α = 102.28 (1)°, β = 114.85 (1)°, γ = 79.41 (1)°, and Z = 2. Final R = 0.033, and final R_w = 0.046.

Introduction

The anionic butterfly Fe_4 carbide cluster in $[PPN]_2[Fe_4(CO)_{12}C]$ (**1**) has a cluster valence electron count of 62 electrons, which is predicted for a butterfly cluster.[1-3] This cluster reacts with the alkylating agents MeI and $PhCH_2Br$ to give $[PPN][Fe_4(CO)_{12}CC(O)Me]$ (**2a**) and $[PPN][Fe_4(CO)_{12}CC(O)CH_2Ph]$ (**2b**), respectively, with the acyl group bonded to the carbide atom (eq 1).[3,4] The clusters **2a** and **2b** have a butterfly symmetry,[5]

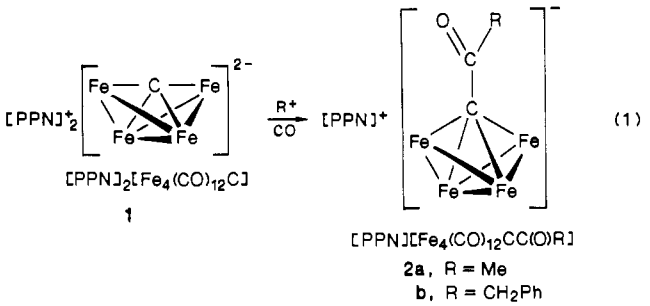

$[PPN]_2[Fe_4(CO)_{12}C]$

1

$[PPN][Fe_4(CO)_{12}CC(O)R]$

2a, R = Me

b, R = CH_2Ph

(1)

but their 60 cluster valence electrons are 2 short of the 62 electrons required for the butterfly structure[1] if the CC(O)R ligand is considered to be a 3-electron donor. Despite the electron count, MO calculations indicate that a satisfactory electron structure can be achieved in these clusters.[5-7] We were prompted to investigate the reduction of **2** to determine whether these clusters behave as if they were indeed electron deficient. Here we report the one-electron reduction that resulted in compounds containing the anions that have the same composition as **2a** and **2b** but are dinegatively charged: $[PPN]_2[Fe_4(CO)_{12}CC(O)Me]$ (**3a**), $[PPN]_2[Fe_4(CO)_{12}CC(O)CH_2Ph]$ (**3b**), and $[Me_3NCH_2Ph]_2[Fe_4(CO)_{12}CC(O)Me]$ (**3c**). The molecular structure of compound **3c** has been determined by a single-crystal X-ray diffraction study.

Experimental Section

Materials and Methods. All reactions were carried out under anhydrous conditions with standard vacuum line and Schlenk techniques.[8] Solvents were dried and distilled prior to use: CH_2Cl_2 from P_2O_5, THF, 2-MeTHF, Et_2O, and $(i\text{-}Pr)_2O$ from sodium benzophenone ketyl, pentane from 4A molecular sieves, and MeOH from Mg/I_2. CH_3CN for electrochemical experiments was distilled from CaH_2, followed by vacuum distillation from P_2O_5 and storage over 4A molecular sieves. Acetyl chloride, alkyl halides, and ethyl acetate were dried and purified by standard procedures.[9] [PPN]Cl (Alfa, $[PPN]^+$ = bis(triphenylphosphine)nitrogen(1+)), $[Me_3NCH_2Ph]Cl$ (Aldrich), Na (Aldrich), and Hg (Goldsmith) were used as received. The electrolyte [*n*-$Bu_4N][BF_4]$ (TBAFB) was recrystallized twice from ethyl acetate/pentane and dried at 60 °C overnight before use. The metal complexes $[PPN]_2[Fe_4(CO)_{12}C]$,[10] $[PPN][Fe_4(CO)_{12}CC(O)CH_3]$,[3] and $[PPN][Fe_4(CO)_{12}CC(O)CH_2Ph]$[4] were synthesized by literature methods.

Instrumentation and Measurements. Cyclic voltammetry and controlled-potential coulometry were performed on a BAS-100 electrochemical analyzer, which is equipped with *iR* feedback circuitry for CV. All of the data reported here are corrected for *iR* drop. Cyclic voltammograms were obtained by using a three-electrode system consisting of a Pt or glassy-carbon (GC) disk working electrode, a Pt-loop counter electrode, and a silver-wire reference electrode. The reference electrode was separated from the bulk solution in a glass tube filled with electrolyte solution and fitted with a porous plug. The reference was corrected to Ag/AgCl by using internal Cp_2Fe. The electrolyte solution for CV was 0.1 M in TBAFB ($[n\text{-}Bu_4N][BF_4]$) and 1 mM in electroactive species. In order to determine the number of electrons transferred in a redox process, controlled-potential coulometry was performed in a two-compartment cell separated by a fine-porosity glass frit, using Pt gauze as the working and counter electrodes.

The EPR measurements were made on a Varian FRAT spectrometer (X-band), which was fitted with a low-temperature accessory. Strong pitch was used as a standard (g = 2.0028 ± 0.0001). The samples were prepared either by controlled-potential coulometry in a 2-MeTHF (2-methyltetrahydrofuran) solution that was 0.075 M in TBAFB and 2 mM in the cluster or by dissolution of the isolated salt of the cluster to make a 2 mM solution in 2-MeTHF. Infrared spectra were recorded on a Perkin-Elmer 283 or 399 spectrophotometer or on a Nicolet 7199 Fourier-transform infrared spectrophotometer. Elemental analyses were performed by Analytische Laboratorien Elbach, Engelskirchen, West Germany.

^{13}C Enrichment of $[PPN][Fe_4(CO)_{12}CC(O)CH_2Ph]$. A sample of $[PPN]_2[Fe_4(CO)_{13}]$ was enriched to ca. 90% ^{13}CO by stirring a dichloromethane solution of the cluster under 99% ^{13}CO for several days, with one change of the ^{13}CO atmosphere during the process. $[PPN]_2[Fe_4(*CO)_{13}]$ was converted to $[PPN]_2[Fe_4(*CO)_{12}*C]$,[10] which was then

† Northwestern University.
‡ Exxon Research and Engineering Co.

(1) Lauher, J. W. *J. Am. Chem. Soc.* **1978**, *100*, 5305-5315.
(2) Boehme, R. F.; Coppens, P. *Acta Crystallogr., Sect. B* **1981**, *B37*, 1914-1916.
(3) Davis, J. H.; Beno, M. A.; Williams, J. H.; Zimmie, J.; Tachikawa, M.; Muetterties, E. L. *Proc. Natl. Acad. Sci. U.S.A.* **1981**, *78*, 668-671.
(4) Bogdan, P. L.; Woodcock, C.; Shriver, D. F. *Organometallics* **1987**, *6*, 1377-1381.
(5) Bradley, J. S.; Harris, S.; Newsam, J. M.; Hill, E. W.; Leta, S.; Modrick, M. *Organometallics* **1987**, *6*, 2060-2069.
(6) Harris, S.; Bradley, J. S. *Organometallics* **1984**, *3*, 1086-1093.
(7) Wijeyesekera, S. D.; Hoffmann, R.; Wilker, C. N. *Organometallics* **1984**, *3*, 962-970.
(8) Shirver, D. F.; Drezdzon, M. A. *The Manipulation of Air-Sensitive Compounds*, 2nd ed.; Wiley: New York, 1986.
(9) (a) Gordon, A. J.; Ford, R. A. *The Chemist's Companion*; Wiley: New York, 1972. (b) Perrin, D. D.; Armarego, W. L. F.; Perrin, D. R. *Purification of Laboratory Chemicals*, 2nd ed.; Pergamon: New York, 1980.
(10) Kolis, J. W.; Drezdzon, M. A.; Shriver, D. F. *Inorg. Synth.*, in press.

0020-1669/89/1328-0697$01.50/0

Table I. Crystallographic Data for Compound **3c**

formula	$C_{35}H_{35}O_{13}N_2Fe_4$	V	1883 (1) Å^3
molar mass	915.06 g	Z	2
space group	$P\bar{1}$	ρ_{calcd}	1.61 g cm^{-3}
a	12.242 (2) Å	T	−120 °C
b	14.904 (3) Å	λ	0.71069 Å
c	11.704 (2) Å	μ	16.18 cm^{-1}
α	102.28 (1)°	transmission coeff	0.73–1.00
β	114.85 (1)°	$R(F_o)$	0.033
γ	79.41 (1)°	$R_w(F_o)$	0.046

stirred with natural isotopic CO to yield $[PPN]_2[Fe_4(CO)_{12}{}^*C]$. This selectively enriched carbide was then converted to $[PPN][Fe_4(CO)_{12}{}^*CC(O)CH_2Ph]$.[4]

Selective enrichment of the terminal CO ligands was accomplished by stirring a dichloromethane solution of $[PPN][Fe_4(CO)_{12}CC(O)CH_2Ph]$ under 99% ^{13}CO for 2 weeks, while the ^{13}CO atmosphere was changed every few days. The level of enrichment was estimated to be 90–95% from infrared spectroscopy.

Synthesis of $[PPN]_2[Fe_4(CO)_{12}CC(O)CH_3]$. In a typical reaction 100 mg of $[PPN][Fe_4(CO)_{12}CC(O)CH_3]$ (0.087 mmol) and 50 mg of [PPN]Cl (0.087 mmol) were dissolved in 10 mL of THF. Dilute sodium/mercury amalgam (ca. 0.043 M in Na) was added to the above solution in increments no larger than 0.5 mL each time, care being taken to exclude air rigorously. The solution was stirred continuously. IR spectra were obtained on the solution at least 10 min after each addition. The reaction was terminated when the CO stretching bands for **2a** at 2040 (w) and 1998 (s) cm^{-1} disappeared or decreased to a minimal intensity. Approximately 2 mL of the amalgam was used. The brown solution was cannulated from the unreacted Hg and filtered from the byproduct NaCl. A crystalline product was obtained by layering diisopropyl ether over the concentrated filtrate in a diffusion tube at −20 °C; isolated yield 63 mg, 43%. Solution IR (THF): ν_{CO} 1976 (s), 1945 (vs), 1925 (sh) cm^{-1}. Solid-state IR (Nujol): ν_{CO} 2006 (w), 1966 (s), 1930 (vs), 1906 (s), 1869 (sh), 1772 (w) cm^{-1}. Anal. Calcd for $C_{87}H_{63}O_{13}N_2P_4Fe_4$: C, 61.76; H, 3.75; N, 1.66; P, 7.32; Fe, 13.20. Found: C, 61.63; H, 3.87; P, 7.44; Fe, 13.15.

Synthesis of $[PPN]_2[Fe_4(CO)_{12}CC(O)CH_2Ph]$. By the procedure described above, $[PPN]_2[Fe_4(CO)_{12}CC(O)CH_2Ph]$ was synthesized when $[PPN][Fe_4(CO)_{12}CC(O)CH_2Ph]$ was reduced with Na/Hg. IR spectra are similar to those for $[PPN]_2[Fe_4(CO)_{12}CC(O)CH_3]$.

Synthesis of $[Me_3NCH_2Ph]_2[Fe_4(CO)_{12}CC(O)CH_3]$. A solution of $[PPN]_2[Fe_4(CO)_{12}CC(O)CH_3]$ in THF was treated with 2 equiv of $K[BPh_4]$ and 2 equiv of $[Me_3NCH_2Ph]Cl$ successively. The resulting solution was cooled to −20 °C, and diisopropyl ether was allowed to diffuse into it to produce single crystals of $[Me_3NCH_2Ph]_2[Fe_4(CO)_{12}CC(O)CH_3]$. A crystal from this batch was used in the X-ray diffraction study described below.

X-ray Data Collection and Structure Determination. All measurements were performed on an Enraf-Nonius CAD4 diffractometer using Mo Kα radiation at −120 °C. The intensities of three standard reflections were measured every 3 h of X-ray exposure, and these showed no significant variation. A summary of crystal and intensity data is presented in Table I. The data were corrected for Lorentz and polarization effects, and an absorption correction was based on a ψ scan of six reflections with the transmission factors range 0.73–1.00.

All calculations were carried out on a VAX 11/730 computer using the TEXSAN crystallographic software package.[11] The structure was solved by heavy-atom techniques (SHELXS 86)[12] and refined by full-matrix least-squares procedures with anisotropic thermal parameters for all non-hydrogen atoms. All H atoms were located from difference Fourier maps and included as fixed contributors to the structure factors. The largest residual peak on the final difference map was 1 Å^3 high. Atomic scattering factors were those from Cromer and Waber[13a] with anomalous dispersion corrections from another table by Cromer.[13b] Final coordinates of all the atoms in the anion are reported in Table II.

Calculations. Molecular orbital calculations with the Fenske–Hall method[14] were carried out for $[Fe_4(CO)_{12}CC(O)CH_3]^{2-}$ in two configurations. The first configuration used atomic coordinates from $[Fe_4(CO)_{12}CC(O)CH_3]^-$,[5] while the second used the coordinates reported in this paper for the dinegative ion of **3c**. All of the basis functions were identical with those used for the earlier calculations for $[Fe_4(CO)_{12}CC(O)CH_3]^-$.[5]

Table II. Positional Parameters with Estimated Standard Deviations for $[Me_3NCH_2Ph]_2[Fe_4(CO)_{12}CC(O)Me]$

atom	x	y	z
Fe(1)	0.26715 (5)	0.34967 (4)	0.27675 (5)
Fe(2)	0.09854 (5)	0.29207 (4)	0.06490 (5)
Fe(3)	0.36827 (5)	0.19437 (4)	0.35468 (5)
Fe(4)	0.31453 (5)	0.21362 (4)	0.12428 (5)
O(1)	0.5029 (3)	0.4003 (2)	0.4659 (3)
O(2)	0.1279 (3)	0.4503 (2)	0.4242 (3)
O(3)	0.2453 (3)	0.5026 (2)	0.1445 (3)
O(4)	0.0388 (3)	0.4295 (2)	−0.1066 (3)
O(5)	−0.0400 (3)	0.1496 (12)	−0.1264 (3)
O(6)	−0.0888 (3)	0.3768 (2)	0.1598 (3)
O(7)	0.3154 (3)	0.2366 (2)	0.5828 (3)
O(8)	0.3962 (3)	−0.0060 (2)	0.3388 (3)
O(9)	0.6311 (3)	0.2021 (3)	0.4823 (3)
O(10)	0.2294 (2)	0.2350 (2)	−0.1421 (3)
O(11)	0.5524 (3)	0.2760 (2)	0.2042 (3)
O(12)	0.3748 (3)	0.0167 (2)	0.0576 (3)
O(13)	0.0684 (2)	0.2122 (2)	0.3033 (3)
C(1)	0.4131 (4)	0.3752 (3)	0.3942 (4)
C(2)	0.1814 (4)	0.4078 (3)	0.3670 (4)
C(3)	0.2508 (4)	0.4403 (3)	0.1912 (4)
C(4)	0.0659 (3)	0.3767 (3)	−0.0388 (4)
C(5)	0.0156 (4)	0.2048 (3)	−0.0505 (4)
C(6)	−0.0142 (4)	0.3442 (3)	0.1234 (4)
C(7)	0.3360 (3)	0.2207 (3)	0.4927 (4)
C(8)	0.3830 (4)	0.0726 (3)	0.3429 (4)
C(9)	0.5295 (4)	0.2004 (3)	0.4299 (4)
C(10)	0.2528 (3)	0.2335 (3)	−0.0350 (4)
C(11)	0.4581 (4)	0.2534 (3)	0.1769 (4)
C(12)	0.3486 (4)	0.0944 (3)	0.0850 (4)
C(13)	0.2072 (3)	0.2270 (2)	0.2154 (3)
C(14)	0.1238 (3)	0.1780 (3)	0.2341 (4)
C(15)	0.1035 (4)	0.0806 (3)	0.1648 (4)
H(15A)	0.0237	0.0747	0.1115
H(15B)	0.1254	0.0415	0.2169
H(15C)	0.1425	0.0528	0.1150

Table III. Cyclic Voltammetry Data for $[PPN][Fe_4(CO)_{12}CC(O)R]$ (R = Me, CH_2Ph)[a]

compd	working electrode	$E_{1/2}$, V	n[b]
R = Me (**2a**)	Pt	−0.38	1
	GC	−0.40	1
R = Bz (**2b**)	Pt	−0.38	1
	GC	−0.41	1

[a] In 0.1 M TBAFB/CH_3CN; scan speed = 200 mV s^{-1}. i_{pa}/i_{pc} = 1.0 in all cases. [b] From controlled-potential coulometry.

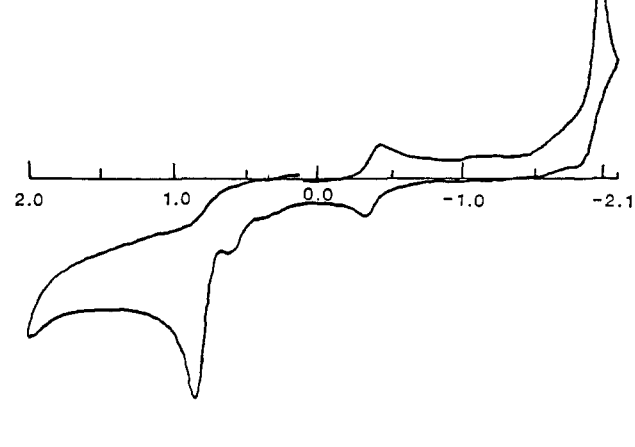

Figure 1. Cyclic voltammogram of $[PPN][Fe_4(CO)_{12}CC(O)CH_2Ph]$ (**2b**) in CH_3CN (Pt working electrode, scan speed 100 mV s^{-1}, Ag/AgCl reference). Compound **2a** gave a CV identical with this one.

(11) Swepston, P. N. "TEXSAN; Version 2.0"; Molecular Structure Corp.: College Station, TX, 1986.
(12) Sheldrick, G. M. "SHELXS 86 Program for Crystal Structure Determination"; University of Göttingen, Göttingen, FRG, 1986.
(13) (a) *International Tables for X-ray Crystallography*; Ibers, J. A., Hamilton, W. C., Eds.; Kynoch: Birmingham, England, 1974; Vol. 4, pp 93–101. (b) *Ibid.*, pp 149–150.
(14) Hall, M. B.; Fenske, R. F. *Inorg. Chem.* **1972**, *11*, 768–775.

Table IV. Variation of ΔE_p with Scan Speed (v)[a]

	ΔE_p, mV			
	compd **2a**		compd **2b**	
v, V s^{-1}	Pt	GC	Pt	GC
0.010	60	60	60	61
0.020	60	65	60	61
0.050	60	70	60	68
0.100	68	76	60	70
0.200	74	92	67	81
0.500	85	97	74	89
1.00	92	104	78	97
2.00	98	112	89	123

[a] In 0.1 M TBAFB/CH_3CN, at 25 °C.

Table V. Heterogeneous Rate Constants for Electron Transfer (k_s(ap), 10^2 cm s^{-1}) for **2a** and **2b** at Pt and GC Electrodes[a]

	2a	**2b**
Pt	2.6 (3)	3.3 (3)
GC	1.2 (2)	1.5 (3)

[a] The values of k_s(ap) are averages of the values calculated at each scan speed. The numbers in parentheses are standard deviations in these numbers.

Results and Discussion

Electrochemistry. The cyclic voltammetry of $[PPN][Fe_4(CO)_{12}CC(O)R]$ (**2a**, R = Me; **2b**, R = CH_2Ph) in acetonitrile at Pt electrodes indicates reduction at −0.38 V vs Ag/AgCl for both **2a** and **2b** (Figure 1). At glassy-carbon (GC) electrodes this potential shifts only slightly from that observed with a Pt electrode (Table III). In addition, several irreversible oxidation processes occur in the cyclic voltammograms. The latter peaks were not studied in detail. The irreversible reduction that takes place at −1.95 V is due to the $[PPN]^+$ counterion.

A controlled-potential electrolysis of the acetyl derivative **2a** in acetonitrile at −0.67 V consumes 0.94 equiv of electrons and changes the color of the solution from dark green-brown to dark brown. The CO stretching bands in the IR spectrum shift to 1978 (s), 1948 (s), and 1927 (sh) cm^{-1} in the reduced species **3a** from 2040 (m) and 1995 (s) cm^{-1} in the starting material **2a**. The IR spectrum of **3a** is very similar to that of $[PPN]_2[Fe_4(CO)_{12}C]$ (**1**), which indicates that **3a** has the same charge (2−) and symmetry as **1**. The bulk electrolysis of the benzyl derivative **2b** proceeds in exactly the same manner. The color also changes from greenish to dark brown, and the solution IR spectrum of the reduced species **3b** in the CO stretching region is the same as that of **3a**. The same redox couple appears in the cyclic voltammograms of the reduced species **3a** and **3b**, but reversing the direction of limited scans shows that the reduced rather than the oxidized species are present. Unsurprisingly, **3a** and **3b** are reoxidized to the starting materials **2a** and **2b**, respectively, at 0.0 V, by passing 0.98 equiv of electrons. After oxidation, the color of the solution changed back to green and the IR spectra back to those for **2a** and **2b**.

For the reduction/oxidation couple at −0.38 V, the peak current ratio, i_{pa}/i_{pc}, remains at 1 for scan rates (v) between 0.01 and 2.00 V s^{-1}. Plots of i_{pc} vs $v^{1/2}$ are linear and intersect the origin of the axes. At fast scan rates, the separations of the peak potentials substantially exceed 60 mV (Table IV), but the value of 60 mV is attained at slow scan rates. This quasi-reversible behavior indicates a moderate rate for the heterogeneous charge transfer at two quite different electrode materials. An estimate of the apparent heterogeneous rate constant, k_s(ap), was obtained by the method of Nicholson,[15] and the results are tabulated in Table V.[16] The values of k_s(ap) of ca. 10^{-2} cm s^{-1} are on the fast end on the range observed for carbonyl clusters.[17] For example, the one-electron reduction of $Co_3(CO)_9(CR)$ takes place with k_s(ap) = ca. 10^{-3} cm s^{-1} at Pt electrodes.[18] The relatively fast rate constant observed for **2a** and **2b** suggests but does not prove that only minor structural reorganization takes place during electron transfer.[19]

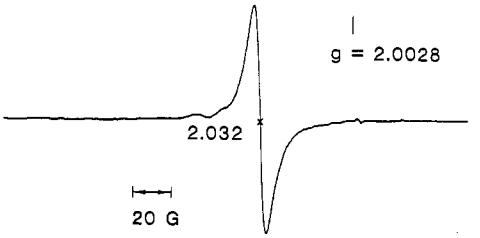

Figure 2. EPR spectrum of **3b** at room temperature in 2-MeTHF. The vertical line at g = 2.0028 marks the position of the resonance of the external standard (strong pitch).

There have been very few reports of definitively reversible one-electron reduction of mononegatively charged organometallic cluster ions. Reversible reduction of $[FeCo_2(CO)_7(\mu\text{-}CO)(\mu\text{-}PPh_2)_2]^-$ was observed at −1.2 V vs SCE only at high scan rate (20 V s^{-1}).[20] The reduction of $[Fe_3(CO)_{12}]^-$ at −0.84 V (vs SCE, CH_2Cl_2 solution) was described to be reversible at scan rates of 0.1 V s^{-1} or higher by some[21] but not fully reversible even at 8 V s^{-1} by others.[22] There are more examples of irreversible reduction of mononegative to dinegative cluster ions, mostly at potentials more negative than −1.2 V.[19,23] Compared to these, the redox potential of −0.38 V for the one-electron reduction of **2a** and **2b** is exceedingly mild. Usually paramagnetic cluster species generated in an electrochemical process are unstable and undergo further redox or decomposition reactions.[19-23] For instance, the cyclic voltammograms of $[Cp_4Fe_4S_5]$ showed potential ranges of existence for the radical 1+ and 1− cluster ions much narrower than those for the diamagnetic 2+ and neutral species.[23] Therefore, the cyclic voltammogram we obtained is remarkable. The mild potential for the reduction of **2a** and **2b**, the reversibility of this reduction, the stability of the reduction product, and the wide potential range for the existence of **3a** and **3b** suggested that these radical 2− cluster ions might be synthesized by chemical reduction.

Synthesis. In view of the electrochemical results, a mild reducing agent, sodium/mercury amalgam, was chosen to chemically reduce **2a** and **2b**. When quantitative amounts of dilute sodium amalgam are added to solutions of **2a** and **2b** in the presence of [PPN]Cl, chemical reduction products **3a** and **3b** are formed, which show IR ν_{CO} bands identical with those of the compounds generated electrochemically (eq 2). The Na/Hg reagent was

$$\underset{\mathbf{2}}{[PPN][Fe_4(CO)_{12}CC(O)R]} \xrightarrow[[PPN]Cl,\ \text{room temp}]{Na/Hg,\ THF} \underset{\mathbf{3}}{[PPN]_2[Fe_4(CO)_{12}CC(O)R]} + NaCl \quad (2)$$

R = Me (**a**), CH_2Ph (**b**)

(15) Nicholson, R. *Anal. Chem.* **1965**, *37*, 1351-1355.
(16) Diffusion coefficients were determined by polarography to be 5.0×10^{-6} cm^2 s^{-1} for **2a** and **2b** by Jacob Saar.
(17) Geiger, W. E. *Prog. Inorg. Chem.* **1985**, *33*, 275-352.
(18) (a) Peake, B. M.; Robinson, B. H.; Simpson, J.; Watson, D. J. *Inorg. Chem.* **1977**, *16*, 405-409. (b) Bond, A. M.; Peake, B. M.; Robinson, B. H.; Simpson, J.; Watson, D. F. *Inorg. Chem.* **1977**, *16*, 410-414. (c) Bond, A. M.; Dawson, P. A.; Peake, B. M.; Rieger, P. H.; Robinson, B. H.; Simpson, J. *Inorg. Chem.* **1979**, *18*, 1413-1417.
(19) Geiger, W. E.; Connelly, N. G. *Adv. Organomet. Chem.* **1985**, *24*, 87-130.
(20) Young, D. A. *Inorg. Chem.* **1981**, *20*, 2049-2054.
(21) El Murr, N.; Chaloyard, A. *Inorg. Chem.* **1982**, *21*, 2206-2208.
(22) Miholova, D.; Klima, J.; Vlcek, A. A. *Inorg. Chim. Acta* **1978**, *27*, L67-L68.
(23) Jordanov, J.; Gaillard, J.; Prudon, M. K.; van der Linden, J. G. M. *Inorg. Chem.* **1987**, *26*, 2202-2205.

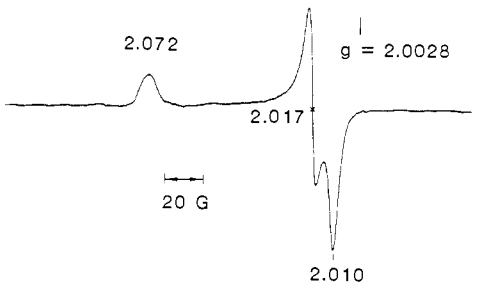

Figure 3. EPR spectrum of **3b** at 120 K in 2-MeTHF. The vertical line at $g = 2.0028$ marks the position of the resonance of the external standard (strong pitch).

added dropwise to prevent local overreduction, and excess Na/Hg was avoided. The reaction was monitored by infrared spectroscopy in the CO stretching region. After addition of each 0.5-mL aliquot of Na/Hg, approximately 10 min was required before the IR spectrum no longer changed.

The reduction products **3a** and **3b** were isolated by crystallization from THF/diisopropyl ether. In solvents such as MeOH, EtOH, and CH_2Cl_2, **3a** and **3b** slowly convert back to **2a** and **2b**; this oxidation is more rapid in air. Cyclic voltammograms and EPR spectra characteristic of the electrochemical product were obtained on samples of crystalline **3a** and **3b** after they were stored under N_2 for an extended time, indicating that these compounds are stable in the solid state in the absence of air.

EPR. Radicals **3a** and **3b** were generated by controlled-potential coulometry in 0.075 M TBAFB/2-MeTHF (saturated solution). The solvent 2-MeTHF was used in place of acetonitrile for the EPR experiments. The EPR spectrum of **3b** at room temperature appears in Figure 2. The spectrum for **3a** is essentially identical with that for **3b** with equal g values. The g values around 2.032 are typical for iron carbonyl radical species.[24-26] The only spin-active nuclei (^1H) in the cluster are on the Me or CH_2Ph groups. Since no hyperfine splitting is observed, the unpaired spin must not be appreciably delocalized over these organic groups. In a glass at low temperature the anisotropy of the g value is manifested in a rhombic type spectrum with three inequivalent g values (Figure 3). These g values are 2.072, 2.017, and 2.010 for **3b** and 2.070, 2.019, and 2.010 for **3a**. The average g values for the low-temperature spectra match (within ±0.001) the room-temperature g values for these samples.

In order to probe the location of the unpaired spin in **3a** and **3b**, the clusters were selectively enriched with ^{13}CO. Upon reduction of the **2b** sample that was ^{13}C-enriched at the bridging carbide C atom only, $[PPN][Fe_4(CO)_{12}{}^*CC(O)CH_2Ph]$, the EPR spectra at 298 and 120 K both appear qualitatively the same as those of the unenriched species. The g values are 2.033 at 298 K and 2.074, 2.016, and 2.007 at 120 K. No hyperfine splitting is resolved, but the peak-to-peak width of the room-temperature resonance increases slightly from 7.7 G in the unenriched sample to 10.5 G in the enriched sample.

The methyl cluster **2a** showed no appreciable enrichment even after prolonged stirring under ^{13}CO. The benzyl cluster **2b** was selectively enriched to 90–95% at the terminal CO ligands. The room-temperature EPR spectrum of the reduced species **3b**, which was derived from ^{13}CO-enriched **2b**, appears in Figure 4. The signal appears as a single broad peak, with a peak-to-peak width of 31.5 G. At a 90–95% level of enrichment, a significant number of species with 12, 11, and 10 ^{13}CO ligands out of the 12 terminal CO ligands will be present in appreciable amounts. If the unpaired spin is equally delocalized over all 12 CO ligands, hyperfine splitting will produce patterns with 13, 12, and 11 lines, which will be superimposed on the same g value. Considering the resolution of the experiment with X-band frequency (9.5 GHz), it is not surprising that the hyperfine splitting could not be resolved. However, broadening of the peaks for the ^{13}C-enriched samples implies a small but finite coupling to the terminal ^{13}CO and the bridging carbide ^{13}C ligands. Since the EPR spectra of the benzoyl and the acetyl derivatives are indistinguishable, and no hyperfine coupling to the protons of the organic groups is observed, the unpaired spin must be delocalized on the metal cluster and not on the $-C(O)Me$ or $-C(O)CH_2Ph$ groups.

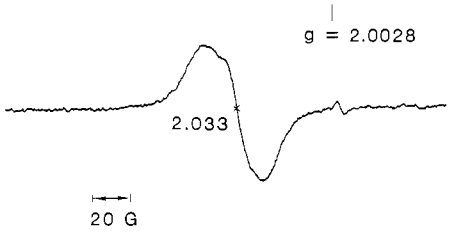

Figure 4. EPR spectrum of $[Fe_4(*CO)_{12}CC(O)CH_2Ph]^{2-}$ at 298 K. The sample was generated from $[PPN][Fe_4(*CO)_{12}CC(O)CH_2Ph]$ with 90–95% ^{13}CO in the metal-bound carbonyls.

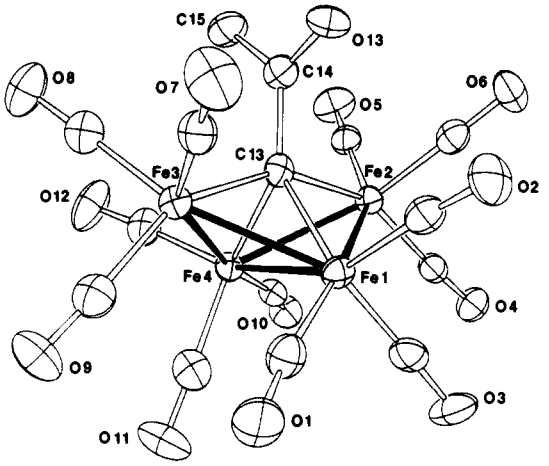

Figure 5. ORTEP diagram of the anion of **3c**, $[Fe_4(CO)_{12}CC(O)Me]^{2-}$. Thermal ellipsoids are drawn at the 50% probability level. Labels for the carbon atoms of the terminal CO ligands can be inferred from numbers on the attached oxygen atoms.

Table VI. Bond Distances (Å) in $[Me_3NCH_2Ph]_2[Fe_4(CO)_{12}CC(O)Me]$ with Estimated Standard Deviations

Fe(1)–Fe(2)	2.5670 (9)	Fe(4)–C(10)	1.761 (4)
Fe(1)–Fe(3)	2.5725 (9)	Fe(4)–C(11)	1.771 (5)
Fe(1)–Fe(4)	2.5556 (8)	Fe(4)–C(12)	1.756 (4)
Fe(2)–Fe(4)	2.5508 (8)	C(1)–O(1)	1.137 (5)
Fe(3)–Fe(4)	2.5604 (8)	C(2)–O(2)	1.147 (5)
Fe(1)–C(13)	1.973 (4)	C(3)–O(3)	1.151 (5)
Fe(2)–C(13)	2.024 (4)	C(4)–O(4)	1.144 (5)
Fe(3)–C(13)	2.016 (4)	C(5)–O(5)	1.147 (5)
Fe(4)–C(13)	1.974 (3)	C(6)–O(6)	1.152 (5)
Fe(1)–C(1)	1.787 (5)	C(7)–O(7)	1.152 (5)
Fe(1)–C(2)	1.782 (4)	C(8)–O(8)	1.147 (5)
Fe(1)–C(3)	1.782 (5)	C(9)–O(9)	1.135 (5)
Fe(2)–C(4)	1.812 (4)	C(10)–O(10)	1.167 (5)
Fe(2)–C(5)	1.770 (4)	C(11)–O(11)	1.157 (5)
Fe(2)–C(6)	1.775 (4)	C(12)–O(12)	1.157 (5)
Fe(3)–C(7)	1.768 (4)	C(13)–C(14)	1.467 (5)
Fe(3)–C(8)	1.771 (4)	C(14)–O(13)	1.239 (5)
Fe(3)–C(9)	1.803 (5)	C(15)–C(14)	1.513 (6)

Crystal Structure. Because the single crystals of **3a** did not diffract sufficiently well for X-ray crystallography, $[Me_3NCH_2Ph]_2[Fe_4(CO)_{12}CC(O)CH_3]$ (**3c**) was prepared from **3a** by metathesis and crystallized to give single crystals suitable for X-ray diffractional measurements. The single-crystal structure of **3c** reveals two $[Me_3NCH_2Ph]$ and one $[Fe_4(CO)_{12}CC(O)CH_3]$ unit in the asymmetric unit of the crystal cell. The bond distances

(24) (a) Krusic, P. J.; San Filippo, J., Jr.; Hutchinson, B.; Hance, R. L.; Daniels, L. M. *J. Am. Chem. Soc.* **1981**, *103*, 2129–2131. (b) Krusic, P. J. *J. Am. Chem. Soc.* **1981**, *103*, 2131–2133.
(25) Muetterties, E. L.; Sosinsky, B. A.; Zamaraev, K. I. *J. Am. Chem. Soc.* **1975**, *97*, 5299–5300.
(26) Lappert, M. F.; MacQuitty, J. J.; Pye, P. L. *J. Chem. Soc., Dalton Trans.* **1981**, 1583–1592.

Table VII. Bond Angles (deg) in $[Me_3NCH_2Ph]_2[Fe_4(CO)_{12}CC(O)Me]$ with Estimated Standard Deviations

Fe(2)–Fe(1)–Fe(3)	99.76 (3)	Fe(4)–C(10)–O(10)	167.5 (3)
Fe(2)–Fe(1)–Fe(4)	59.73 (2)	Fe(4)–C(11)–O(11)	175.6 (4)
Fe(3)–Fe(1)–Fe(4)	59.91 (2)	Fe(4)–C(12)–O(12)	177.1 (4)
Fe(1)–Fe(2)–Fe(4)	59.91 (2)	C(1)–Fe(1)–C(2)	97.4 (2)
Fe(1)–Fe(3)–Fe(4)	59.72 (2)	C(1)–Fe(1)–C(3)	94.3 (2)
Fe(1)–Fe(4)–Fe(2)	60.36 (2)	C(2)–Fe(1)–C(3)	98.0 (2)
Fe(1)–Fe(4)–Fe(3)	60.38 (2)	C(4)–Fe(2)–C(5)	98.2 (2)
Fe(2)–Fe(4)–Fe(3)	100.52 (3)	C(4)–Fe(2)–C(6)	94.5 (2)
Fe(1)–C(13)–Fe(2)	79.9 (1)	C(5)–Fe(2)–C(6)	97.8 (2)
Fe(1)–C(13)–Fe(3)	80.3 (1)	C(7)–Fe(3)–C(8)	96.8 (2)
Fe(1)–C(13)–Fe(4)	80.7 (1)	C(7)–Fe(3)–C(9)	98.7 (2)
Fe(2)–C(13)–Fe(3)	153.2 (2)	C(8)–Fe(3)–C(9)	93.5 (2)
Fe(2)–C(13)–Fe(4)	79.3 (1)	C(10)–Fe(4)–C(11)	99.6 (2)
Fe(3)–C(13)–Fe(4)	79.8 (1)	C(10)–Fe(4)–C(12)	93.9 (2)
Fe(1)–C(1)–O(1)	173.1 (4)	C(11)–Fe(4)–C(12)	101.3 (2)
Fe(1)–C(2)–O(2)	175.7 (3)	Fe(1)–C(13)–C(14)	136.6 (3)
Fe(1)–C(3)–O(3)	174.9 (4)	Fe(2)–C(13)–C(14)	103.5 (2)
Fe(2)–C(4)–O(4)	176.3 (3)	Fe(3)–C(13)–C(14)	103.3 (2)
Fe(2)–C(5)–O(5)	178.6 (4)	Fe(4)–C(13)–C(14)	142.7 (3)
Fe(2)–C(6)–O(6)	178.7 (4)	C(13)–C(14)–O(13)	123.5 (3)
Fe(3)–C(7)–O(7)	179.1 (4)	C(13)–C(14)–C(15)	118.5 (3)
Fe(3)–C(8)–O(8)	177.7 (4)	C(15)–C(14)–O(13)	118.0 (3)
Fe(3)–C(9)–O(9)	176.4 (4)		

Table VIII. Comparison of Structural Data for **1**,[a] **2a**,[b] and **3c**[c]

	$[Fe_4C]^{2-}$ (anion of **1**)	$[Fe_4CC(O)Me]^-$ (anion of **2a**)	$[Fe_4CC(O)Me]^{2-}$ (anion of **3c**)
	Distances (Å)		
Fe(1)–Fe(4)	2.533 (2)	2.572 (1)	2.5556 (8)
Fe(1)–Fe(2)	2.621 (2)	2.507 (1)	2.5670 (9)
Fe(1)–Fe(3)	2.654 (2)	2.519 (1)	2.5725 (9)
Fe(4)–Fe(2)	2.637 (2)	2.501 (1)	2.5508 (8)
Fe(4)–Fe(3)	2.630 (2)	2.504 (1)	2.5604 (8)
Fe_h–Fe_w (av)[d]	2.636	2.508	2.5627
Fe–Fe (av)	2.615	2.521	2.5613
Fe_h–C(13)	1.96 ± 0.02	1.97 ± 0.01	1.97 ± 0.01
Fe_w–C(13)	1.80 ± 0.02	2.01 ± 0.01	2.02 ± 0.01
smallest Fe···C[e]	2.943	2.736	2.552 (4)
	Angles (deg)		
Fe(2)–C(13)–Fe(3)	176.3 (4)	148.6 (2)	153.2 (2)
butterfly dihedral[f]	102	128	124
smallest Fe–C–O	174.6	171.6 (7)	167.5 (3)

[a] Reference 2; $[Zn(NH_3)_4]^{2+}$ salt. [b] Reference 5; $[Et_4N]^+$ salt. [c] Present work; $[Me_3NCH_2Ph]^+$ salt. A consistent atom-numbering scheme is used for all three clusters. In the case of **1**, the numbering differs from that in the original publication.[2] [d] Fe_h = Fe atom at a hinge position; Fe_w = Fe atom at a wingtip position. [e] Distance from a wingtip Fe atom to the C atom of the CO ligand on a neighboring hinge Fe atom. [f] Dihedral angle between the two planes, each of which is defined by the hinge Fe atoms and one wingtip Fe atom.

and angles for the anion $[Fe_4(CO)_{12}CC(O)CH_3]^{2-}$ of **3c** are presented in Tables VI and VII.

As is shown in the ORTEP diagram (Figure 5), the anion of **3c** consists of four Fe atoms in a butterfly framework; the hinge irons are designated as Fe(1) and Fe(4) and the wingtips as Fe(2) and Fe(3). Three CO groups are attached to eachh Fe atom; the carbide carbon atom of the $CC(O)CH_3$ group is situated between and above the two wingtip irons. Although the anion in **3c** is dinegative, its molecular structure more closely resembles that of the mononegative analogue **2a** than it does the dinegative cluster anion in **1**, $[Fe_4(CO)_{12}C]^{2-}$ (Table VIII). For instance, the butterfly clusters in both **3c** and **2a** are more open (dihedral angles Fe(2)–Fe(1)–Fe(4)–Fe(3) = 124 and 128°, respectively) than in compound **1** (102°). For compound **1** the carbide atom sits only 0.06 Å above the two wingtip Fe atoms, while the carbide atoms in **3c** and **2a** are substantially above the Fe(2)–Fe(3) vector (0.47 and 0.56 Å, respectively). The resulting Fe(2)–C(13)–Fe(3) angles are 153.2 (2), 148.6 (2), and 176.3 (4)° for **3c**, **2a**, and **1**, respectively. The effect of the acetyl group on the carbide in the $[Fe_4C]$ cluster is to push back the wingtip Fe atoms of the butterfly so that the Fe_w–C(13) distances become longer and the butterfly dihedral angle becomes larger (Table VIII). The butterfly dihedral

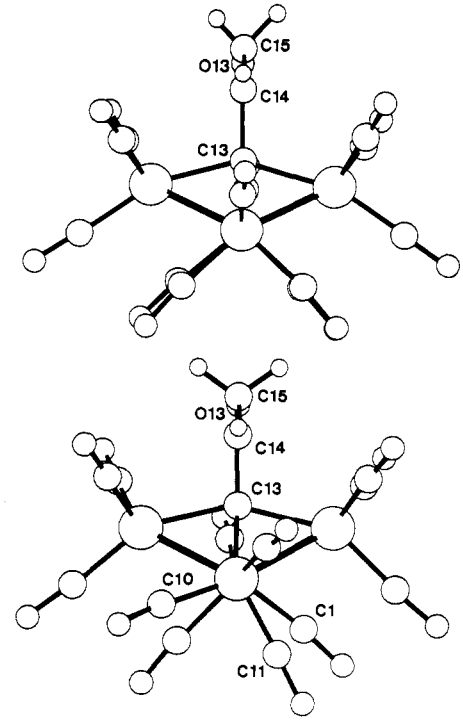

Figure 6. Views along the hinge Fe–Fe bonds of the butterfly cluster anions of (top) **2a**, $[Fe_4(CO)_{12}CC(O)Me]^-$, and of (bottom) **3c**, $[Fe_4(CO)_{12}CC(O)Me]^{2-}$.

angle, the Fe(2)–C(13)–Fe(3) angle, and the Fe–Fe distances for the cluster anion of **3c** are all intermediate between those for the anions of **1**, $[Fe_4(CO)_{12}C]^{2-}$, and of **2a**, $[Fe_4(CO)_{12}CC(O)Me]^-$.

Comparison between the structures of **3c** and **2a** is of interest to determine the influence of reduction on bond distances and angles of the cluster. The structure of the $CC(O)CH_3$ group in **3c** is essentially the same as in **2a** within experimental error.[5] By contrast, major differences are evident between the $[Fe_4(CO)_{12}]$ cluster groups of **3c** and **2a** (Table VIII). Reduction leads to a slight shortening of the hinge Fe–Fe distance and significant elongation of the hinge-to-wingtip Fe–Fe distances. Also, substantial changes occur in the CO disposition; for example, CO(10) on Fe(4) is bent (Fe(4)–C(10)–O(10) = 167.5 (3)°) and it approaches Fe(2) (Fe(2)–C(10) = 2.552 (4) Å), to which it is not directly bound. Although CO(1) on Fe(1) is still reasonably linear (Fe(1)–C(1)–O(1) = 173.1 (4)°), it approaches Fe(3) slightly (Fe(3)–C(1) = 2.753 (5) Å). These changes in CO orientation can be viewed as a rotation of the three CO ligands on each hinge iron atom in **3c** away from their original disposition in **2a** (Figure 6). The changes in Fe–Fe bond distances and terminal CO disposition are consistent with EPR data, indicating that the extra electron is on the $[Fe_4(CO)_{12}]$ moiety and not the $CC(O)CH_3$ ligand.

Electronic Structure. As has been outlined above, the reduction from **2** to **3** causes lengthening of the butterfly hinge-to-wingtip Fe–Fe distances and apparent semibridging of a CO ligand on the hinge iron, CO(10), to a wingtip iron atom. The description of the bonding in the butterfly Fe_4 carbide clusters and their derivatives has been established by Fenske–Hall and extended Hückel molecular orbital calculations.[5-7] Bradley and Harris have compared the structures of $[Fe_4(CO)_{12}CC(O)R]^-$ (R = CH_3, OCH_3) with that of $[Fe_4(CO)_{12}C]^{2-}$ and commented on the geometry of the Fe_4 butterfly framework.[5,6] The invariable geometry of the $[Fe_4C]$ core in $[Fe_4(CO)_{12}C]^{2-}$, $[HFe_4(CO)_{12}C]^-$, and $Fe_4(CO)_{13}C$ was described in terms of strong interactions between all three carbon 2p orbitals and orbitals on the wingtip Fe atoms.[5-7] This invariance is no longer observed for the –C(O)R derivatives. The Fe_w atoms fold back and away from the carbide C(13) atom, increasing the dihedral angle between the two "wings" of the butterfly and shortening the Fe_w–Fe_h bond distances. These changes in geometry result in weaker Fe_w–C(13) bonds but stronger Fe_w–Fe_h bonds. In contrast with this previous work, the

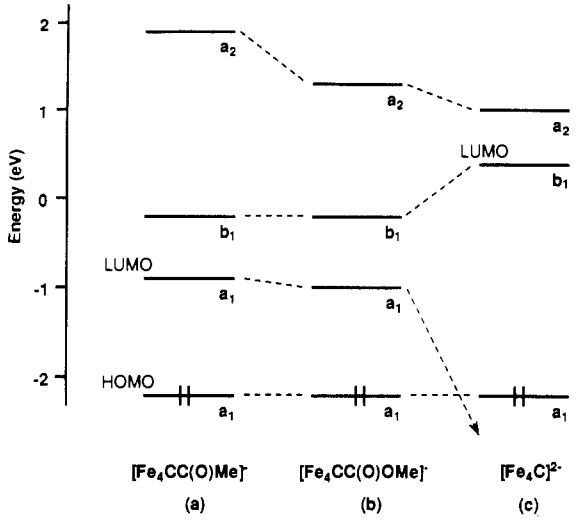

Figure 7. Calculated energies for the HOMO and low-energy unoccupied orbitals in (a) $[Fe_4(CO)_{12}CC(O)Me]^-$ (anion of **2a**), (b) $[Fe_4(CO)_{12}CC(O)OMe]^-$,[6] and (c) $[Fe_4(CO)_{12}C]^{2-}$ (anion of **1**).[6] All energies are scaled relative to that of **2a**, and the HOMO's in all the clusters are placed at the same energy. To aid in the comparisons, the symmetry labels for the C_{2v} point group are used throughout.

present discussion focuses on the low-energy unoccupied molecular orbital that accommodates the electron added upon reduction.

Comparison of frontier orbitals of $[Fe_4(CO)_{12}CC(O)CH_3]^-$, $[Fe_4(CO)_{12}CC(O)OCH_3]^-$,[6] and $[Fe_4(CO)_{12}C]^{2-}$ reveals that the LUMO in $[Fe_4(CO)_{12}C]^{2-}$ differs from the LUMO in both –C(O)R derivatives. Figure 7c shows that in $[Fe_4(CO)_{12}C]^{2-}$ the LUMO has b_1 symmetry and lies about 2.6 eV above the HOMO, whereas for the two –C(O)R derivatives (Figure 7a,b) a new LUMO having a_1 symmetry lies ~1.2–1.3 eV above the HOMO. A schematic representation of this LUMO is shown in I. It is

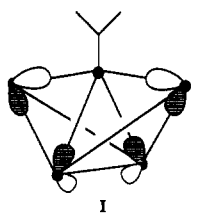

I

weakly antibonding between the wingtip and hinge Fe atoms and contains considerably more wingtip than hinge metal orbital character. The contribution of orbitals from the acyl ligand is negligible. The occurrence of this orbital in the derivatized clusters is related to the weaker interaction between the wingtip Fe atoms and the carbide C atom. In $[Fe_4(CO)_{12}C]^{2-}$, the corresponding "a_1" metal framework orbital participates in π-bonding with the carbide carbon p_z orbital, so that its energy falls below the frontier levels. In the derivatized clusters, this "a_1" orbital remains in the frontier region because the longer Fe_w–C(13) distances and the involvement of the p_z orbital in C–C bonding eliminate the Fe_w–C π-bonding. Since this orbital is weakly antibonding between the hinge and wingtip Fe atoms, addition of an electron should weaken but not break the Fe_h–Fe_w bonding. This is consistent with the lengthening of the Fe_h–Fe_w bonds observed upon reduction of **2a**.

To further explore the influence of the added electron on Fe_h–Fe_w bonding and cluster geometry, two sets of Fenske–Hall molecular orbital calculations[14] were carried out on the dinegative cluster ion. In the first calculation, the structure of the cluster was assumed to be identical with the structure of the 1– anion in **2a**. The extra electron occupies the orbital shown in I. This added electron has little effect on Fe–C(13) bonding, but as expected, it weakens the Fe_h–Fe_w bonds. This is indicated by the reduction in the Fe_h–Fe_w overlap populations (Table IX). By contrast, the Fe_h–Fe_h overlap population is unchanged. Thus, the calculated change in electronic structure is consistent with the observed lengthening of Fe_h–Fe_w bond distances upon addition of an electron to $[Fe_4(CO)_{12}CC(O)CH_3]^-$.

Table IX. Fe–Fe Overlap Populations for **1**,[a] **2a**,[b] and **3c**

	$[Fe_4C]^{2-}$ (anion of **1**)	$[Fe_4CC(O)Me]^-$ (anion of **2a**)	$[Fe_4CC(O)Me]^{2-}$ (anion of **3c**)
Fe_h–Fe_h	0.075	0.058	(0.059)[c] 0.055
Fe_h–Fe_w (av)	0.036	0.058	(0.046)[c] 0.042

[a] Reference 6. [b] Reference 5. [c] Values in parentheses were calculated for the 2– anion in the configuration of the 1– anion.

The second calculation on the dinegative ion was based on the actual coordinates for the anion in **3c**, determined in the present work. In comparison with the calculations based on the structure of **2a**, the charge distribution and molecular orbitals are virtually unchanged, but small decreases are evident in all of the Fe–Fe overlap populations. The decrease in Fe_h–Fe_w overlap population comes about from the longer Fe_h–Fe_w distances. There is little change in Fe_h–Fe_h distance, however, and the decrease in overlap population between the hinge Fe atoms is probably related to the twist of the $(CO)_3$ arrays on the hinge Fe atoms.

Orientation of Carbonyl Ligands. The above calculations do not provide a ready electronic explanation for the rotation of the $(CO)_3$ array on the hinge Fe atoms. Although the short distances between C(10) and Fe(2) in compound **3c** might result from a semibridging interaction, calculated orbital overlap populations show no net bonding between CO(10) and Fe(2). These results suggest that the $(CO)_3$ reorientation in **3c** is probably dictated by steric rather than electronic effects. In an earlier study,[5] the structure of $[Fe_4(CO)_{12}CC(O)CH_3]^-$ was compared with that of $[Fe_4(CO)_{12}CC(O)OCH_3]^-$. The CC(O)R group in the former cluster is tilted within the plane defined by Fe(1), Fe(4), and C(13) away from Fe(4), while no such tilt is observable in the latter. Small adjustments in the disposition of the CO ligands on the metal framework accompany the tilt of the CC(O)R group. Molecular mechanics calculations on those clusters suggested that both the tilt of the acetyl group and the adjustments of the cluster carbonyls tend to accommodate the bulk of the CC(O)R group. It was shown that these adjustments do not disrupt the Fe–C(13) bonding.[5] In the present study we find that the tilt angle in **3c** is actually *smaller* than in **2a** (3 versus 5°, respectively). The steric repulsion with CO groups on the hinge appears to be relieved in **3c** by rotation of the hinge-bound $(CO)_3$ array.

Conclusion. The reversible one-electron reduction of $[PPN][Fe_4(CO)_{12}CC(O)R]$ (**2a**, R = Me; **2b**, R = CH_2Ph) to $[PPN]_2[Fe_4(CO)_{12}CC(O)R]$ (**3a**, R = Me; **3b**, R = CH_2Ph) has been carried out at an unusually favorable potential and with dilute Na/Hg. In view of the ease of reduction and stability of the radical products, compounds **2a** and **2b** behave as if they are electron deficient. The EPR spectra of **3a** and **3b** show hyperfine coupling of the unpaired electron to the terminal carbonyls and the carbide C atom but not to the –C(O)R ligand attached to the carbide. Similarly, the X-ray single-crystal structure of $[Me_3NCH_2Ph]_2[Fe_4(CO)_{12}CC(O)Me]$ (**3c**) reveals longer hinge to wingtip Fe–Fe bond distances than in **2a** but no major change in the CC(O)Me ligand. The ease of reduction, EPR spectra, and structural data are readily explained by an MO treatment, which reveals a low-energy unoccupied orbital that is present in clusters of the type $[Fe_4(CO)_{12}CC(O)R]^-$ but absent in $[Fe_4(CO)_{12}C]^{2-}$. This orbital is mainly metal based and is weakly antibonding between hinge and wingtip iron atoms. Another structural change resulting from the reduction is the rotation of a $(CO)_3$ array on one hinge Fe atom. This is attributed to steric interactions with the capping CC(O)R group and not to electronic effects.

Acknowledgment. Dr. Paula L. Bogdan provided samples of **2a** and **2b** as well as inspiration for the initial electrochemical study. Dr. Jacob Saar helped in analyzing the kinetic implication of the preliminary cyclic voltammograms.[16] J.W. also thanks C. K. Schauer, M. J. Sailor, and S. Ching for helpful suggestions.

The portion of this research carried out at Northwestern University was supported by the NSF Synthetic Inorganic Organometallic Program (Grant No. CHE 8506011).

Supplementary Material Available: For the crystal structure of **3c**, listings of all thermal parameters, additional positional parameters, additional bond distances and angles, selected torsion angles, and selected intermolecular distances and a summary of crystal structure data (17 pages); a complete listing of observed and calculated structure factors (31 pages). Ordering information is given on any current masthead page.

Contribution from the Department of Chemistry, University of South Carolina, Columbia, South Carolina 29208

Cluster Synthesis. 24. Synthesis and Characterization of New Sulfur-Containing Tungsten–Iron Carbonyl Cluster Complexes

Richard D. Adams,* James E. Babin, Jin-Guu Wang, and Wengan Wu[1]

Received September 29, 1988

The reaction of $Fe_3(CO)_9(\mu_3\text{-}S)_2$ (**1**) with $W(CO)_6$ under UV irradiation yielded the $W(CO)_5$ adduct, $Fe_3(CO)_9(\mu_3\text{-}S)(\mu_4\text{-}S)[W(CO)_5]$ (**3**), formed by the addition of the $W(CO)_5$ group to one of the sulfido ligands in **1**. The reaction of **1** with $W(CO)_5(PMe_2Ph)$ under UV irradiation yielded the related PMe_2Ph derivative of **3**, $Fe_3(CO)_9(\mu_3\text{-}S)(\mu_4\text{-}S)[W(CO)_4PMe_2Ph]$ (**5**), but also two new products $WFe_2(CO)_9(PMe_2Ph)(\mu_3\text{-}S)_2$ (**6**) and $WFe_3(CO)_{11}(PMe_2Ph)(\mu_3\text{-}S)_2$ (**7**). Compound **7** can be obtained by UV irradiation of **5**. Compound **6** can be obtained from **7** in low yield by reaction with CO but was obtained in a better yield (40%) from the reaction of $Fe_2(CO)_6(\mu\text{-}S_2)$ (**2**) with $W(CO)_5(PMe_2Ph)$ in the presence of UV irradiation. This reaction also yielded a $W(CO)_5$ adduct of **6**, $WFe_2(CO)_9(PMe_2Ph)(\mu_3\text{-}S)(\mu_4\text{-}S)[W(CO)_5]$ (**8**), in very low yield, 3%. Compound **8** was obtained in 37% yield from the reaction of **6** with $W(CO)_6$ under UV irradiation. Compounds **5**–**8** were characterized by X-ray crystallographic methods. For **5**: space group *Pnma*, a = 24.033 (6) Å, b = 14.226 (4) Å, c = 8.715 (4) Å, Z = 4; solved by direct methods with R = 0.028 for 1579 reflections. For **6**: space group $P2_1/n$, a = 9.129 (1) Å, b = 15.878 (6) Å, c = 16.208 (3) Å, β = 91.52 (1)°, Z = 4; solved by direct methods with R = 0.029 for 2477 reflections. For **7**: space group $P\bar{1}$, a = 10.751 (2) Å, b = 13.776 (3) Å, c = 9.424 (3) Å, α = 101.55 (2)°, β = 98.67 (2)°, γ = 76.34 (1)°, Z = 2; solved by direct methods with R = 0.024 for 4069 reflections. For **8**: space group $C2/c$, a = 29.91 (1) Å, b = 13.427 (3) Å, c = 17.640 (5) Å, β = 120.48 (2)°, Z = 8; solved by direct methods with R = 0.027 for 3418 reflections. The structure of **6** consists of an open WFe_2 cluster with two W–Fe bonds and triply bridging sulfido ligands on opposite sides of the cluster. The structure of **7** consists of a butterfly WFe_3 cluster with the tungsten atom in a hinge position. Sulfido ligands bridge the two closed Fe_2W triangular groups on opposite sides of the cluster. Compounds **5** and **8** are $W(CO)_4L$ adducts of **1**, L = PMe_2Ph, and **6**, L = CO, respectively. The transformation of **5** to **7** is evidence that the sulfido ligand plays a key role in the metal-addition and cluster-forming processes. It is also believed that the lower electron density withdrawal capacity of the PMe_2Ph ligand compared to that of CO is one feature that promotes the stabilization of the W–Fe bonds observed in **6** and **7**.

Introduction

Bridging ligands derived from the elements of the main groups have been found to play an important role, both in the synthesis and in the stabilization of transition-metal cluster complexes.[2-7] Much of our recent research has been focused on systematics of the synthesis, structure, and bonding of sulfur-containing carbonyl clusters of ruthenium[8-10] and osmium.[7] We have shown that the sulfido ligand can promote the agglomerization of metal atoms by readily expanding its coordination number. Two examples of this are shown by eq 1[11] and 2.[8-10] By the first route, sulfur uses its lone pair of electrons to donate to an empty orbital on a metal-containing group M′ (A). In this reaction, no metal–metal bonds are formed. The sulfido ligand has a pseudotetrahedral geometry and serves as a neutral six-electron donor. By the second route, the metal-containing group is inserted into a metal–metal bond of the sulfido cluster B. Two metal–metal bonds and one

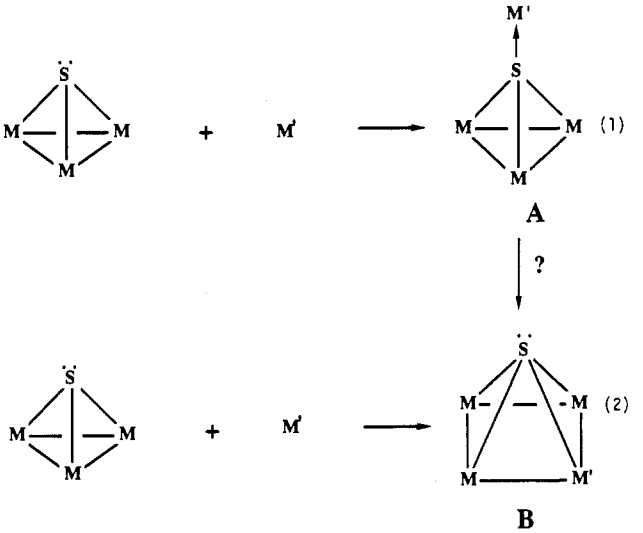

metal–sulfur bond are formed, and the square-pyramidal sulfido ligand serves as a four-electron donor. Species such as A could be key intermediates in the formation of B, but this has not yet been established.

We have previously investigated the reactions of $Os_3(CO)_9(\mu_3\text{-}S)_2$ with $W(CO)_6$ and $W(CO)_5PMe_2Ph$.[11,12] In this report is described our investigation of the reactions of $Fe_3(CO)_9(\mu_3\text{-}S)_2$

(1) Visiting Scholar on leave from Zhenjiang Teacher's College, Zhenjiang, Jiangsu, People's Republic of China.
(2) Whitmire, K. H. *J. Coord. Chem.* **1988**, *17*, 95.
(3) (a) Huttner, G.; Knoll, K. *Angew. Chem., Int. Ed. Engl.* **1987**, *26*, 743. (b) Huttner, G.; Evertz, K. *Acc. Chem. Res.* **1986**, *19*, 406.
(4) Roberts, D. A.; Geoffroy, G. L. In *Comprehensive Organometallic Chemistry*; Wilkinson, G., Stone, F. G. A., Abel, E., Eds.; Pergamon: Oxford, England, 1982; Chapter 40.
(5) Vahrenkamp, H. *Angew. Chem., Int. Ed. Engl.* **1975**, 322.
(6) Gourdin, A.; Jeannin, Y. J. *Organomet. Chem.* **1986**, *304*, C1.
(7) Adams, R. D. *Polyhedron* **1985**, *4*, 2003.
(8) (a) Adams, R. D.; Babin, J. E.; Tasi, M. *Inorg. Chem.* **1986**, *25*, 4514. (b) Adams, R. D.; Babin, J. E.; Tasi, M. *Inorg. Chem.* **1987**, *26*, 2807.
(9) Adams, R. D.; Babin, J. E.; Tasi, M. *Organometallics* **1988**, *7*, 503.
(10) Adams, R. D.; Babin, J. E.; Tasi, M. *Inorg. Chem.* **1986**, *25*, 4460.
(11) Adams, R. D.; Horvath, I. T.; Wang, S. *Inorg. Chem.* **1985**, *22*, 1728.
(12) Adams, R. D.; Horvath, I. T.; Mathur, P. *J. Am. Chem. Soc.* **1984**, *106*, 6292.

0020-1669/89/1328-0703$01.50/0